Aging in the Long-Range Ising Model

Henrik Christiansen,[1,*] Suman Majumder,[1,†] Malte Henkel,[2,3,4,‡] and Wolfhard Janke[1,§]
[1]Institut für Theoretische Physik, Universität Leipzig, IPF 231101, 04081 Leipzig, Germany
[2]Laboratoire de Physique et Chimie Théoriques (CNRS UMR 7019), Université de Lorraine Nancy, 54506 Vandœuvre-lès-Nancy Cedex, France
[3]Centro de Física Teórica e Computacional, Universidade de Lisboa, 1749-016 Lisboa, Portugal
[4]Max-Planck-Institut für Physik komplexer Systeme, Nöthnitzer Straße 38, 01187 Dresden, Germany

(Received 27 June 2019; revised 1 August 2020; accepted 10 September 2020; published 28 October 2020)

The current understanding of aging phenomena is mainly confined to the study of systems with short-ranged interactions. Little is known about the aging of long-ranged systems. Here, the aging in the phase-ordering kinetics of the two-dimensional Ising model with power-law long-range interactions is studied via Monte Carlo simulations. The dynamical scaling of the two-time spin-spin autocorrelator is well described by simple aging for all interaction ranges studied. The autocorrelation exponents are consistent with $\lambda = 1.25$ in the effectively short-range regime, while for stronger long-range interactions the data are consistent with $\lambda = d/2 = 1$. For very long-ranged interactions, strong finite-size effects are observed. We discuss whether such finite-size effects could be misinterpreted phenomenologically as subaging.

DOI: 10.1103/PhysRevLett.125.180601

The time evolution of complex systems after a quench from a disordered state at high temperature to a low temperature where the equilibrium state has a nonzero order parameter is characterized by dynamical scaling laws describing coarsening and aging phenomena [1–4]. Understanding this nonequilibrium phase-ordering kinetics is key for predicting structure formation processes in many fields. Applications range from statistical and soft-matter physics at mesoscopic scales [5–15] to biology [16,17], from quantum physics at the nanoscale [18–22] to astrophysics [23–26] at the cosmic scale. In many of these systems, an important role is played by long-range interactions [27–34], which are hard to deal with theoretically and computationally. For aging of long-range interacting systems, comparatively little is known theoretically, with the notable exception of analytical studies of the long-range spherical model [35,36].

In this Letter, we therefore strive to uncover the most distinguishing features of aging of long-range interacting systems when compared to the short-range case. To avoid distractions from system-specific details as much as possible, we consider the paradigmatic two-dimensional (2D) long-range Ising model (LRIM), with Hamiltonian

$$\mathcal{H} = -\frac{1}{2}\sum_i \sum_{j\neq i} J(r_{ij}) s_i s_j \quad \text{and} \quad J(r_{ij}) = \frac{1}{r_{ij}^{d+\sigma}}. \tag{1}$$

The interaction strength $J(r_{ij})$ depends on the distance r_{ij} between the spins at sites i and j that take values $s_i = \pm 1$. The exponent σ governing the power-law decay enables us to interpolate between the short-range nearest-neighbor Ising model (NNIM) over intermediate-range to extremely long-range interactions, encompassing all interaction patterns encountered in nature.

For quenches of the LRIM into the ordered phase at temperatures T below the critical temperature T_c, the system's long-time behavior is characterized by the existence of a single time-dependent length scale, $\ell(t)$, where for phase-ordering kinetics in *any* dimension it has been predicted that [37–39]

$$\ell(t) \propto t^{1/z} = \begin{cases} t^{\frac{1}{1+\sigma}} & \sigma < 1 \\ (t \ln t)^{1/2} & \sigma = 1 \\ t^{\frac{1}{2}} & \sigma > 1 \end{cases}, \tag{2}$$

with z denoting the dynamical exponent [40]. In Fig. 1, we show an illustration with $\sigma = 0.6$, where $\ell(t)$ has been

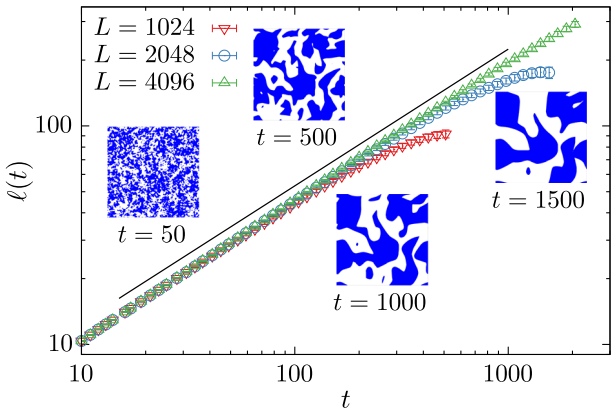

FIG. 1. Characteristic length scale $\ell(t)$ versus time t for the 2D LRIM with $\sigma = 0.6$ on $L \times L$ lattices quenched to $T = 0.1T_c$. The solid line depicts the theoretical prediction in Eq. (2). The snapshots are obtained from a single run for $L = 4096$, with spins pointing up marked in blue.

extracted as the distance where the equal-time two-point correlation function has decayed to 50% (for details see the Supplemental Material [41]).

For a proper understanding of the nonequilibrium process, along with single-time quantities one needs to study multiple-time quantities as well, which provide information about the change in properties of a system with its growing age, i.e., its aging characteristics. Here, this is probed via the two-time autocorrelation function

$$C(t, t_w) = \langle \psi(\vec{r}, t)\psi(\vec{r}, t_w)\rangle, \tag{3}$$

where ψ is the space- and time-dependent order parameter, and t_w ($\leq t$) is the waiting time. In our case, the order parameter is given as $\psi(\vec{r}, t) = s_i(t)$. Simple aging for quenches to $T < T_c$ is characterized [4] by slow dynamics, absence of time-translation invariance and dynamical scaling in the scaling variable $y \equiv t/t_w$. In general, for large y one expects

$$C(yt_w, t_w) = f_C(y) \overset{y\to\infty}{\longrightarrow} f_{C,\infty} y^{-\lambda/z}, \tag{4}$$

where λ is the autocorrelation exponent. It was assumed that $t_w \gg t_{\text{micro}}$ and $t - t_w \gg t_{\text{micro}}$, where t_{micro} is some microscopic reference timescale.

For the NNIM, a lower bound $\lambda \geq d/2$ [5,47] exists. Most simulations [4,48–52] in 2D are compatible with $\lambda \approx 1.25$, and it has been argued that $\lambda \leq 1.25$ [5]. For the LRIM, it is *a priori* unclear if this bound should also apply. Equation (2) suggests that, for $\sigma > 1$, the nonequilibrium behavior might be in the same universality class as the NNIM. If that should be the case, the autocorrelation exponent $\lambda \approx 1.25$ is expected. No prediction for λ exists for $\sigma \leq 1$.

We study the phase-ordering kinetics of the LRIM on $L \times L$ periodic lattices via Monte Carlo simulations by quenching to $T = 0.1T_c(\sigma)$; for details see the Supplemental Material [41]. The values of $T_c(\sigma)$ are from recent equilibrium studies of this model focusing on the critical regime [53]. The unit of time t is one Monte Carlo sweep, corresponding to $L \times L$ randomly drawn spin-flip attempts. All presented results are averaged over at least 30 independent realizations. The error bars are of the order of the size of the data symbols if not shown.

The long-standing theoretical prediction, Eq. (2), for $\ell(t)$ has only recently been confirmed by us in 2D [54] and subsequently in 1D [55]. In Fig. 1, we plot $\ell(t)$ versus t for $\sigma = 0.6$ and $L = 1024$, 2048 [54] and add new data for $L = 4096$. Clear finite-size effects are seen, such that for $t > t_\times(L)$ deviations from the infinite system occur. We estimate the onset of finite-size effects as $t_\times(1024) \approx$ 100–200 and $t_\times(2048) \approx$ 300–500. The exemplary snapshots from a single run illustrate how the emergent structures grow with time.

We now focus on the main part of this Letter: The two-time correlator $C(yt_w, t_w)$. When plotted against $t - t_w$, we get curves that relax slower with increasing t_w, implying the absence of time-translation invariance as shown in the Supplemental Material [41]. We start our quantitative analysis for a case for which we expect behavior similar to the NNIM, i.e., the 2D LRIM in the short-range regime with $\sigma = 1.5$. In Fig. 2(a), we test for dynamical scaling by plotting $C(yt_w, t_w)$ for $L = 2048$ against y on a log-log scale for different waiting times t_w. The data collapse well onto a

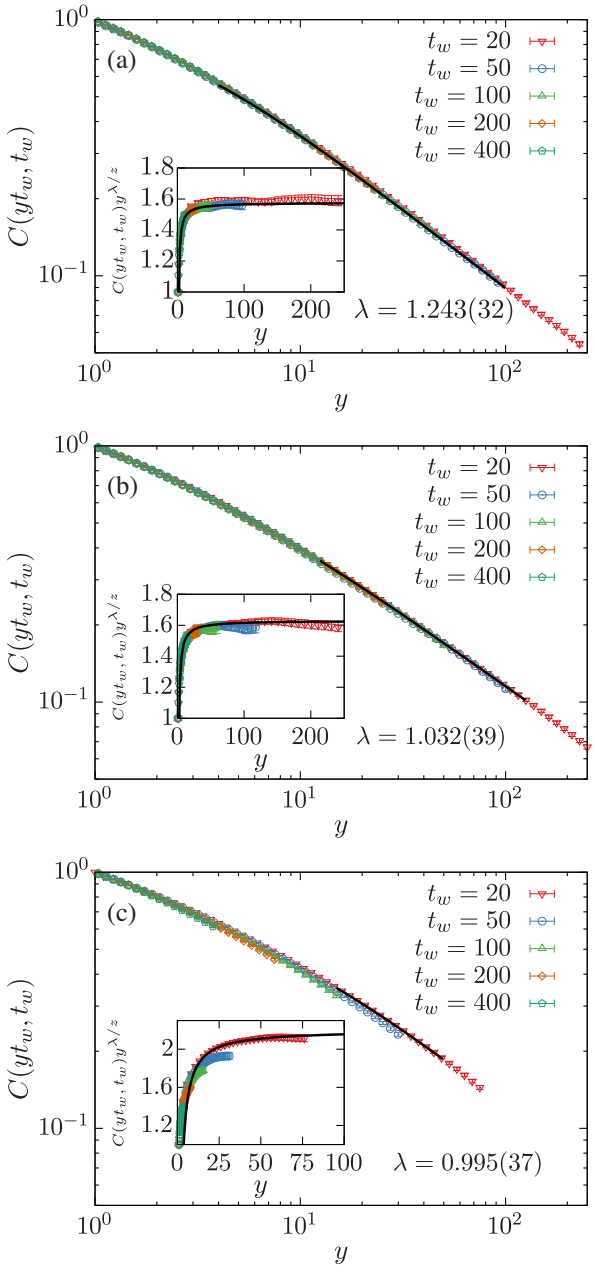

FIG. 2. Double-log plot of the order-parameter autocorrelation function $C(yt_w, t_w)$ against the scaling variable $y = t/t_w$ for the 2D LRIM with (a) $\sigma = 1.5$ with $L = 2048$ and (b) $\sigma = 0.8$ and (c) $\sigma = 0.6$ with $L = 4096$ quenched to $T = 0.1T_c$. The solid lines are fits using Eq. (5). In the insets, we plot the same data on a linear scale but divide out the asymptotic behavior $y^{-\lambda/z}$.

master curve $f_C(y)$, which clearly validates the simple scaling scenario. For small y, we observe a curvature indicating corrections to the asymptotic power law [Eq. (4)], which we assume to be in leading order of the form

$$C(yt_w, t_w) = f_{C,\infty} y^{-\lambda/z}\left(1 - \frac{A}{y}\right). \tag{5}$$

This is a generic ansatz, which is known from the exactly solved spherical [4,35,36] and 1D Glauber-Ising [4] models. More generally, this is also known from local scale invariance [4,56–58] for any phase-ordering system with $z = 2$, where it can also be shown that $A \geq d - \lambda$; see the Supplemental Material [41]. When fitting this ansatz to the data points, we first systematically vary the lower $t_{\min}$ and upper $t_{\max}$ boundaries of the fit window. Out of the resulting 100–200 fits, we select a particular fit by demanding $\Delta t = t_{\max} - t_{\min}$ to be maximal under the constraint that the reduced chi-square χ_r^2 (chi-square per degree of freedom) has no (strong) systematic trend. Effectively, $t_{\min}$ thus indicates down to which t the data are well described by the first-order correction A/y and $t_{\max}$ detects the onset of noticeable finite-size effects. Since the data are (trivially) correlated in time, the value of χ_r^2 has no absolute interpretation, but a comparison of different fitting ranges is still meaningful. All fits in the region where χ_r^2 has no clear trend only show a systematic variation within 1%–2% for λ. Statistical errors on the fit parameters were estimated from a Jackknife analysis [59], i.e., we performed an independent fit for each Jackknife bin (containing all but data from one seed). For $\sigma = 1.5$, we have chosen the data for $t_w = 50$ for our analysis, since small deviations from the master curve are visible for $t_w = 20$. This corresponds to a value of $\ell(t_w) = 12.51(2)$, which is clearly in the scaling regime. In this case, the lower bound is $t_{\min} = 200$ and the upper bound is $t_{\max} = 5000$, where this is the last available data point (i.e., up to this point there are no detectable finite-size effects; see the Supplemental Material [41]). For this fit window, we find $\lambda = 1.243(32)$, $A = 0.67(11)$, and $f_{C,\infty} = 1.566(68)$. This is perfectly consistent with $\lambda = 1.25$ as expected for the NNIM. The solid line in Fig. 2(a) shows this fit restricted to its range of validity from $t_{\min}$ to $t_{\max}$ (for $\sigma = 1.5$ the largest available time t). For $t_w = 50$ this range corresponds to $y_{\min} = 4$ and $y_{\max} = 100$. For how the fit extrapolates to larger and smaller y, see Fig. S4 in the Supplemental Material [41]. In the inset, we plot the same data with the asymptotically expected power law $y^{-\lambda/z}$ divided out, which implies a constant behavior in the asymptotic limit. From the pronounced curvature for small y, the $1/y$ correction in Eq. (5) to the asymptotic power law, Eq. (4), is evident. The solid line shows again the fit, here plotted over the full y range.

Next, we consider the case $\sigma = 0.8$. According to Eq. (1), this should be distinct from the short-range universality class. Our analysis follows the method developed above for $\sigma = 1.5$. In Fig. 2(b), we show the autocorrelation $C(yt_w, t_w)$ for $L = 4096$ as a function of y, which collapses onto a master curve for all shown t_w. Here, we use the data with $t_w = 20$ for our fits, as this provides the longest possible fitting ranges and $\ell(t_w) = 11.90(2)$ is in the scaling regime and compatible with $\ell(t_w)$ used for $\sigma = 1.5$. Fits using Eq. (5) show no systematic trend in the range from $t_{\min} = 250$ to $t_{\max} = 2500$, giving estimates of the fit parameters as $\lambda = 1.032(39)$, $A = 0.88(56)$, and $f_{C,\infty} = 1.63(16)$. Note that the estimate for λ is compatible with $\lambda = d/2 = 1$, the (putative) lower bound on λ. In the phase-ordering long-range spherical model, one also finds $\lambda = d/2$ [35,36]. The quality of the fit is visually reinforced by the solid lines in the main plot and the inset. Here $t_{\max}$ is understood as an estimator for $t_\times$, the time where detectable finite-size effects set in. Data for $t > t_\times$ decay faster than the assumed asymptotic power for all t_w (see the Supplemental Material [41]). In general, these finite-size effects always occur at the same value of $t_\times$, thus effectively at different y. From the inset we see a deviation from the trend of the data for $t_w = 20$ at $y \approx 150$, which indicates that all data for $t \gtrapprox 3000$ need to be disregarded, compatible with $t_\times = 2500$ estimated from the fits.

In contrast, for the data with $\sigma = 0.6$ and $L = 4096$ shown in Fig. 2(c), one observes two problems: (*i*) there is apparently no completely satisfactory data collapse and (*ii*) there is no pronounced power-law-like scaling regime. Performing fits using Eq. (5) for $t_w = 20$ [with $\ell(t_w) = 16.27(3)$] suggests $t_{\max} = 1000$, while $t_{\min} = 300$ appears suitable as a lower bound. This gives $\lambda = 0.995(37)$, $A = 2.02(40)$, and $f_{C,\infty} = 2.20(20)$, which is once more consistent with $\lambda = d/2 = 1$. However, since Δt is rather short and the visual impression of the data collapse is not perfect, we analyze this case in more detail.

Using $t_{\max} = 1000$ as the estimate for $t_\times$, we replot in Fig. 3(a) the data by omitting all points with $t > t_\times$, giving a much improved impression of data collapse. The estimate for $t_\times$ is thus crucial for the visual judgment. To substantiate this, we now estimate the onset of finite-size effects from the data of $\ell(t)$ shown in Fig. 1 in a more dependable way. For this, we plot in the inset of Fig. 3(a) $\ell(t)/t^{1/z}$ versus $t^{1/z}/L$. The onset of finite-size effects in this representation is independent of L and happens at the same value of $t^{1/z}/L$. Here one could read off values of $t_\times^{1/z}/L$ between ≈ 0.012 and ≈ 0.020, corresponding for $L = 4096$ to the relatively wide range $510 \lessapprox t_\times \lessapprox 1150$, compatible with $t_\times$ extracted from the trends of χ_r^2. The straight line in Fig. 3(a) shows $y^{-\lambda/z}$ with $\lambda = 0.995$ from the fit. In Fig. 3(b), we plot $C(yt_w, t_w)y^{\lambda/z}$ against $1/y$, emphasizing the asymptotic behavior when compared to the insets of Fig. 2. For the correct λ the data should approach $f_{C,\infty}$ linearly as $1/y \to 0$. If λ is too large, the data diverge for $1/y \to 0$, whereas for a λ too small, a downward tendency

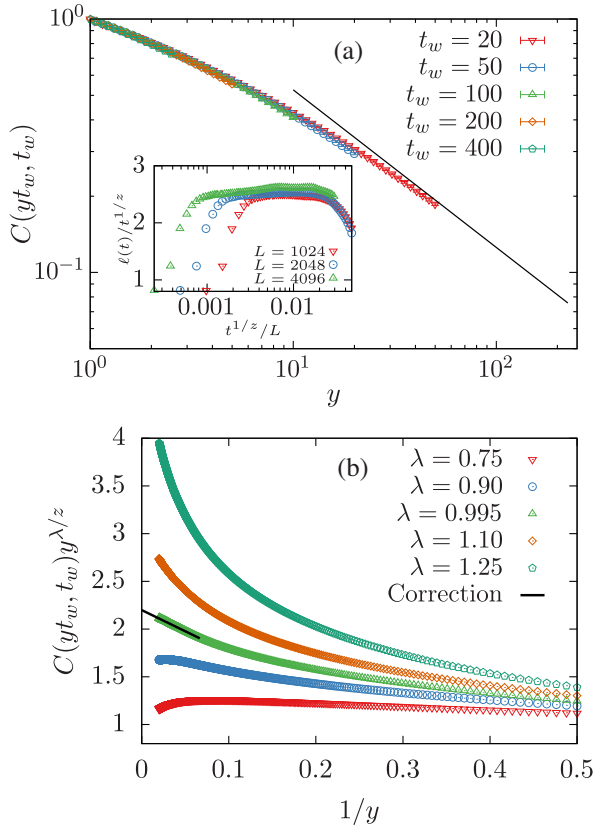

FIG. 3. Autocorrelator scaling function for $\sigma = 0.6$ and $L = 4096$. (a) $C(yt_w, t_w)$ versus y, omitting the finite-size affected data for $t > t_\times = 1000$. The straight line shows the asymptotic power law $y^{-\lambda/z}$ with the fitted $\lambda = 0.995$. The inset shows a finite-size scaling plot of $\ell(t)$ by plotting $\ell(t)/t^{1/z}$ versus $t^{1/z}/L$ for different L. (b) Plot against $1/y$ of the data for $t_w = 20$, dividing out the asymptotically expected behavior of $y^{-\lambda/z}$. The assumed value of λ is varied and the solid line is the expected behavior assuming the correction form in Eq. (5).

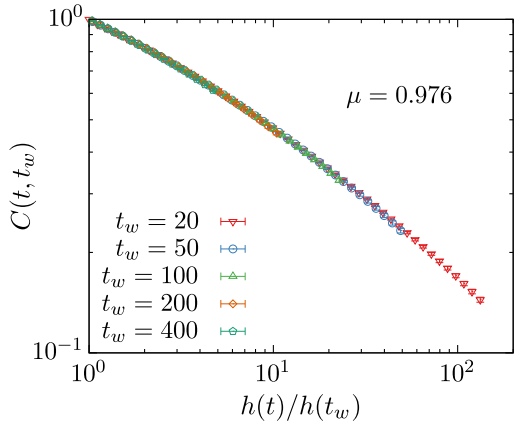

FIG. 4. Untruncated $C(yt_w, t_w)$ for $\sigma = 0.6$ and $L = 4096$ plotted against scaling variable $h(t)/h(t_w)$ with $\mu = 0.976$, indicating subaging.

is expected. From the plot, we observe for $\lambda < 0.995$ this downward tendency, while for $\lambda > 0.995$ the curves have increasing slopes. For $\lambda = 0.995$ the approach to $1/y \to 0$ is indeed linear, with a constant slope over a significant range, which is verified by the solid line as obtained from the fit. For an enlarged plot with a smaller $1/y$-range and λ values closer to 0.995, see the Supplemental Material [41].

We should point out, however, that our current data for $\sigma = 0.6$ would also be compatible with the alternative interpretation of exhibiting subaging behavior. In this scenario, one considers the scaling ansatz

$$C(t, t_w) = \tilde{f}_C\left(\frac{h(t)}{h(t_w)}\right), \tag{6}$$

with $h(t) \equiv \exp\left((t^{1-\mu} - 1)/(1-\mu)\right)$, where the parameter μ characterizes the deviation from simple scaling, which is recovered in the limit $\mu \to 1$. Subaging with $\mu < 1$ has been encountered many times in analytical [13,60], numerical [61–64], and experimental investigations (see Ref. [4] for a list of examples). In Fig. 4, we show the scaling with respect to $h(t)/h(t_w)$ for the untruncated data, where $\mu \approx 0.976$ provides the best data collapse. Compared to Fig. 2(c) showing the same data, the data collapse is greatly improved. Of course, subaging introduces one additional tunable parameter and as such one would always expect better data collapse. On the other hand, we have provided rather strong evidence that the (slight) downward bending of the curves in Fig. 2(c) for large y is caused by finite-size effects [cf., Fig. S2(c) of the Supplemental Material [41]]. Assuming asymptotically $C(t, t_w) \to [h(t)/h(t_w)]^{-\tilde{\lambda}/z}$, where $\tilde{\lambda}$ is a modified autocorrelation exponent, one finds that, for large y (or t for fixed t_w), the subaging ansatz (6) decays faster than any power law, i.e., proportional to $\exp\left(-[(\tilde{\lambda}/z)/(1-\mu)]t^{1-\mu}\right)$. When plotted as a function of y as in Fig. 2(c), this thus models a downward bending, suggesting that the subaging scaling collapse just looks so good because this ansatz effectively "compensates" the finite-size effects. Only on the basis of the present data for $\sigma = 0.6$ on lattices up to 4096×4096 is it, however, not possible to clearly favor one of the two alternative scaling scenarios. Based on our results for the other values of σ where we have clear evidence for simple aging, we side with the interpretation of simple aging also for $\sigma = 0.6$. The Supplemental Material [41] presents, alternatively, the scaling behavior with respect to t/t_w^μ, a simpler phenomenological form often used to probe for subaging.

To conclude, we have performed the first numerical investigation of aging in long-range systems by systematically tuning the interaction range using the paradigmatic two-dimensional long-range Ising model. We find for all σ simple aging, where for $\sigma = 0.6$ it is shown that strong finite-size effects may be misinterpreted as subaging. The autocorrelation exponent is consistent with $\lambda = d/2 = 1$

for $\sigma < 1$ and with $\lambda = 1.25$ for $\sigma > 1$. This implies that the transition between the short-range and long-range 2D Ising universality classes occurs at a different value of σ than it does either *at* the critical point or else in equilibrium. The conjecture $\lambda = d/2$ is consistent with known results. For the 1D LRIM at $T = 0$, one finds $\lambda = 0.5$ for $\sigma < 1$ [65], and the phase-ordering long-range spherical model has $\lambda = d/2$ independently of σ [35,36].

An open and interesting question relates to how this transition in λ happens, i.e., whether it is smooth or is characterized by a jump. To answer this, even larger systems would have to be simulated, which is out of scope for the time being. The more involved case of binary mixtures, i.e., a conserved order parameter setting, is enticing as a next step [66]. Crucial also is the investigation of aging in other models with long-range interactions, as this could shed new light on our understanding of aging in liquid crystals [67], active systems [68], or strongly interacting quantum many-body systems [69].

This project was funded by the Deutsche Forschungsgemeinschaft (DFG, German Research Foundation) under Grants No. JA 483/33-1 and 189 853 844–SFB/TRR 102 (Project B04), and the Deutsch-Französische Hochschule (DFH-UFA) through the Doctoral College "$\mathbb{L}^4$" under Grant No. CDFA-02-07. We further acknowledge support by the Leipzig Graduate School of Natural Sciences "BuildMoNa." M. H. thanks the MPI-PKS Dresden for warm hospitality.

*Corresponding author.
henrik.christiansen@itp.uni-leipzig.de
†suman.majumder@itp.uni-leipzig.de
‡malte.henkel@univ-lorraine.fr
§wolfhard.janke@itp.uni-leipzig.de

[1] J.-P. Bouchaud, Aging in glassy systems: Experiments, models and open questions, in *Soft and Fragile Matter: Nonequilibrium Dynamics, Metastability and Flow*, edited by M. Cates and M. Evans (IOP, Bristol, 2000), p. 285.
[2] A. J. Bray, Theory of phase-ordering kinetics, Adv. Phys. **51**, 481 (2002).
[3] *Kinetics of Phase Transitions*, edited by S. Puri and V. Wadhawan (CRC Press, Boca Raton, 2009).
[4] M. Henkel and M. Pleimling, *Non-Equilibrium Phase Transitions: Ageing and Dynamical Scaling far from Equilibrium* (Springer, Heidelberg, 2010), Vol. 2 (2nd edition expected to be published in 2021).
[5] D. S. Fisher and D. A. Huse, Nonequilibrium dynamics of spin glasses, Phys. Rev. B **38**, 373 (1988).
[6] R. Mathieu, P. Nordblad, D. N. H. Nam, N. X. Phuc, and N. V. Khiem, Short-range ferromagnetism and spin-glass state in $Y_{0.7}Ca_{0.3}MnO_3$, Phys. Rev. B **63**, 174405 (2001).
[7] H. E. Castillo, C. Chamon, L. F. Cugliandolo, and M. P. Kennett, Heterogeneous Aging in Spin Glasses, Phys. Rev. Lett. **88**, 237201 (2002).
[8] P. Lunkenheimer, R. Wehn, U. Schneider, and A. Loidl, Glassy Aging Dynamics, Phys. Rev. Lett. **95**, 055702 (2005).
[9] A. Röthlein, F. Baumann, and M. Pleimling, Symmetry-based determination of space-time functions in non-equilibrium growth processes, Phys. Rev. E **74**, 061604 (2006); Erratum, Phys. Rev. E **76**, 019901 (2007).
[10] M. Henkel, J. Noh, and M. Pleimling, Phenomenology of aging in the Kardar–Parisi–Zhang equation, Phys. Rev. E **85**, 030102(R) (2012).
[11] S. Majumder and W. Janke, Evidence of aging and dynamic scaling in the collapse of a polymer, Phys. Rev. E **93**, 032506 (2016).
[12] J. Kelling, G. Ódor, and S. Gemming, Local scale-invariance of the $2+1$ dimensional Kardar–Parisi–Zhang model, J. Phys. A **50**, 12LT01 (2017).
[13] X. Durang and M. Henkel, Exactly solvable models of growing interfaces and lattice gases: The Arcetri models, ageing and logarithmic sub-ageing, J. Stat. Mech. (2017) 123206.
[14] S. Majumder, J. Zierenberg, and W. Janke, Kinetics of polymer collapse: Effect of temperature on cluster growth and aging, Soft Matter **13**, 1276 (2017).
[15] H. Christiansen, S. Majumder, and W. Janke, Coarsening and aging of lattice polymers: Influence of bond fluctuations, J. Chem. Phys. **147**, 094902 (2017).
[16] M. Costa, A. L. Goldberger, and C.-K. Peng, Broken Asymmetry of the Human Heartbeat: Loss of Time Irreversibility in Aging and Disease, Phys. Rev. Lett. **95**, 198102 (2005).
[17] Y. Lou, J. Xia, W. Tang, and Y. Chen, Linking biological and physical aging: Dynamical scaling of multicellular regeneration, Phys. Rev. E **96**, 062418 (2017).
[18] G. M. Schütz and S. Trimper, Relaxation and aging in quantum spin systems, Europhys. Lett. **47**, 164 (1999).
[19] J. Hofmann, S. S. Natu, and S. Das Sarma, Coarsening Dynamics of Binary Bose Condensates, Phys. Rev. Lett. **113**, 095702 (2014).
[20] H. Jeong, Y. Lim, and M. S. Kim, Coarsening Measurement References and the Quantum-to-Classical Transition, Phys. Rev. Lett. **112**, 010402 (2014).
[21] A. Maraga, A. Chiocchetta, A. Mitra, and A. Gambassi, Aging and coarsening in isolated quantum systems after a quench: Exact results for the quantum $O(N)$ model with $N \to \infty$, Phys. Rev. E **92**, 042151 (2015).
[22] A. Mitra, Quantum quench dynamics, Annu. Rev. Condens. Matter Phys. **9**, 245 (2018).
[23] T. W. B. Kibble, Some implications of a cosmological phase transition, Phys. Rep. **67**, 183 (1980).
[24] E. Witten, Cosmic separation of phases, Phys. Rev. D **30**, 272 (1984).
[25] A. Vilenkin, Cosmic strings and domain walls, Phys. Rep. **121**, 263 (1985).
[26] J. Binney and S. Tremaine, *Galactic Dynamics* (Princeton University Press, Princeton, 2011).
[27] G. L. Eyink and K. R. Sreenivasan, Onsager and the theory of hydrodynamic turbulence, Rev. Mod. Phys. **78**, 87 (2006).
[28] A. Campa, T. Dauxois, and S. Ruffo, Statistical mechanics and dynamics of solvable models with long-range interactions, Phys. Rep. **480**, 57 (2009).
[29] R. H. French, V. A. Parsegian, R. Podgornik, R. F. Rajter, A. Jagota, J. Luo, D. Asthagiri, M. K. Chaudhury, Y. M.

Chiang, S. Granick *et al.*, Long range interactions in nanoscale science, Rev. Mod. Phys. **82**, 1887 (2010).
[30] Y. Levin, R. Pakter, F. B. Rizzato, T. N. Teles, and F. P. C. Benetti, Nonequilibrium statistical mechanics of systems with long-range interactions, Phys. Rep. **535**, 1 (2014).
[31] A. Campa, T. Dauxois, D. Fanelli, and S. Ruffo, *Physics of Long-Range Interacting Systems* (Oxford Scholarship, Oxford, 2014).
[32] J. S. Douglas, H. Habibian, C.-L. Hung, A. V. Gorshkov, H. J. Kimble, and D. E. Chang, Quantum many-body models with cold atoms coupled to photonic crystals, Nat. Photonics **9**, 326 (2015).
[33] B. Neyenhuis, J. Zhang, P. W. Hess, J. Smith, A. C. Lee, P. Richerme, Z. Gong, A. V. Gorshkov, and C. Monroe, Observation of prethermalization in long-range interacting spin chains, Sci. Adv. **3**, e1700672 (2017).
[34] Y.-C. Zhang, V. Walther, and T. Pohl, Long-Range Interactions and Symmetry Breaking in Quantum Gases through Optical Feedback, Phys. Rev. Lett. **121**, 073604 (2018).
[35] S. Cannas, D. Stariolo, and F. Tamarit, Dynamics of ferromagnetic spherical spin models with power law interactions: Exact solution, Physica (Amsterdam) **294A**, 362 (2001).
[36] F. Baumann, S. Dutta, and M. Henkel, Kinetics of the long-range spherical model, J. Phys. A **40**, 7389 (2007).
[37] A. J. Bray, Domain-growth scaling in systems with long-range interactions, Phys. Rev. E **47**, 3191 (1993).
[38] A. J. Bray and A. D. Rutenberg, Growth laws for phase ordering, Phys. Rev. E **49**, R27 (1994).
[39] A. D. Rutenberg and A. J. Bray, Phase-ordering kinetics of one-dimensional nonconserved scalar systems, Phys. Rev. E **50**, 1900 (1994).
[40] In general, one has $\ell(t) \propto t^{\alpha}$, where in most cases $\alpha = 1/z$. However, there exist systems such as fluid mixtures incorporating hydrodynamic effects, where this is not true.
[41] See Supplemental Material at http://link.aps.org/supplemental/10.1103/PhysRevLett.125.180601, which includes Refs. [42–46]. The Supplemental Material contains an introduction to the methods used, an explicit illustration of the loss of time-translational invariance and the finite-size effects, simple-aging plots with a longer range of the fitted form, and a replot of Fig. 3(b) with a smaller $1/y$ range. Furthermore, we present plots with an alternative form of subaging and discuss two-time autocorrelators from local scale invariance with $z = 2$.
[42] P. Ewald, Die Berechnung optischer und elektrostatischer Gitterpotentiale, Ann. Phys. (Berlin) **369**, 253 (1921).
[43] E. Flores-Sola, M. Weigel, R. Kenna, and B. Berche, Cluster Monte Carlo and dynamical scaling for long-range interactions, Eur. Phys. J. Spec. Top. **226**, 581 (2017).
[44] W. Janke, H. Christiansen, and S. Majumder, Coarsening in the long-range Ising model: Metropolis versus Glauber criterion, J. Phys. Conf. Ser. **1163**, 012002 (2019).
[45] S. N. Majumdar and D. A. Huse, Growth of long-range correlations after a quench in phase-ordering systems, Phys. Rev. E **52**, 270 (1995).
[46] G. Brown, P. A. Rikvold, M. Sutton, and M. Grant, Evolution of speckle during spinodal decomposition, Phys. Rev. E **60**, 5151 (1999).
[47] C. Yeung, M. Rao, and R. C. Desai, Bounds on the decay of the autocorrelation in phase ordering dynamics, Phys. Rev. E **53**, 3073 (1996).
[48] M. Zannetti, Aging in domain growth, in *Kinetics of Phase Transitions*, edited by S. Puri and V. Wadhawan (CRC Press, Boca Raton, 2009), p. 153.
[49] M. Henkel, A. Picone, and M. Pleimling, Two-time autocorrelation function in phase-ordering kinetics from local scale invariance, Europhys. Lett. **68**, 191 (2004).
[50] E. Lorenz and W. Janke, Numerical tests of local scale invariance in ageing q-state Potts models, Europhys. Lett. **77**, 10003 (2007).
[51] S. Majumder and S. K. Das, Effects of Density Conservation and Hydrodynamics on Aging in Nonequilibrium Processes, Phys. Rev. Lett. **111**, 055503 (2013).
[52] J. Midya, S. Majumder, and S. Das, Aging in ferromagnetic ordering: Full decay and finite-size scaling of autocorrelation, J. Phys. Condens. Matter **26**, 452202 (2014).
[53] T. Horita, H. Suwa, and S. Todo, Upper and lower critical decay exponents of Ising ferromagnets with long-range interaction, Phys. Rev. E **95**, 012143 (2017).
[54] H. Christiansen, S. Majumder, and W. Janke, Phase ordering kinetics of the long-range Ising model, Phys. Rev. E **99**, 011301(R) (2019).
[55] F. Corberi, E. Lippiello, and P. Politi, One dimensional phase-ordering in the Ising model with space decaying interactions, J. Stat. Phys. **176**, 510 (2019).
[56] M. Henkel, Schrödinger invariance and strongly anisotropic critical systems, J. Stat. Phys. **75**, 1023 (1994).
[57] A. Picone and M. Henkel, Local scale-invariance and ageing in noisy systems, Nucl. Phys. **B688**, 217 (2004).
[58] M. Henkel, From dynamical scaling to local scale-invariance: A tutorial, Eur. Phys. J. Spec. Top. **226**, 605 (2017).
[59] B. Efron, *The Jackknife, the Bootstrap and Other Resampling Plans* (Society for Industrial and Applied Mathematics, Philadelphia, 1982).
[60] L. Berthier, Sub-aging in a domain growth model, Eur. Phys. J. B **17**, 689 (2000).
[61] E. Kim, B. Kim, and S. J. Lee, Nonequilibrium critical dynamics of the triangular antiferromagnetic Ising model, Phys. Rev. E **68**, 066127 (2003).
[62] D. Grempel, Off-equilibrium dynamics of the two-dimensional Coulomb glass, Europhys. Lett. **66**, 854 (2004).
[63] A. Pluchino, V. Latora, and A. Rapisarda, Glassy dynamics in the HMF model, Physica (Amsterdam) **340A**, 187 (2004).
[64] F. Tamarit and C. Anteneodo, Relaxation and aging in a long-range interacting system, Europhysics News **36**, 194 (2005).
[65] F. Corberi, E. Lippiello, and P. Politi, Universality in the time correlations of the long-range 1d Ising model, J. Stat. Mech. (2019) 074002.
[66] (to be published).

[67] A. Singh, S. Ahmad, S. Puri, and S. Singh, Ordering kinetics in liquid crystals with long-ranged interactions, Eur. Phys. J. E **37**, 2 (2014).

[68] J. P. Steimel, J. L. Aragones, H. Hu, N. Qureshi, and A. Alexander-Katz, Emergent ultra-long-range interactions between active particles in hybrid active-inactive systems, Proc. Natl. Acad. Sci. U.S.A. **113**, 4652 (2016).

[69] B. Blaß, H. Rieger, G. Roósz, and F. Iglói, Quantum Relaxation and Metastability of Lattice Bosons with Cavity-Induced Long-Range Interactions, Phys. Rev. Lett. **121**, 095301 (2018).